Auxiliary material for Paper 2004JE002305R
Shock Properties of H_2O Ice

Sarah T. Stewart* and Thomas J. Ahrens
Lindhurst Laboratory of Experimental Geophysics, California Institute of Technology, Pasadena, California, USA

Journal of Geophysical Research-Planets

Submitted June, 2004; Revised, October, 2004; Accepted, November 2004.

Experiment Release Wave Geometry

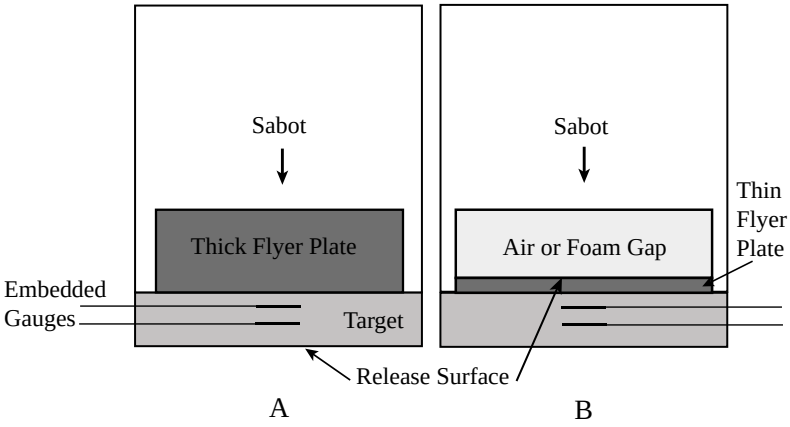

Figure S1. Schematic cross section of experiment geometry for shock loading and release from (A) the downrange face of the sample and (B) the rear surface of the flyer plate.

The experiment geometry defines the primary release process in the shocked sample (Fig. S1). For planar wave shock compression via impact, the shocked sample is released via: (A) Reflection of the shock wave from the downrange free surface of the sample. If the release wave propagates back to a particle velocity gauge position, the Lagrangian particle velocity will begin to increase. (B) After the impact, a shock wave propagates rearward into the projectile, e.g., a planar flyer plate. Upon reflection at the rear surface of the flyer plate, the release wave propagates forward into the sample and decreases the particle velocity as recorded at the embedded gauges.

In the present experiment geometry, the sample is released from the downrange free surface (geometry A). The data from *Gaffney and Smith* [1994] and *Davies and Smith* [1994] record the stress profiles during release from the rear of the flyer plate (geometry B), and *Larson* [1984] measured the particle velocity increase from release from the downrange sample face (geometry A). In *Anderson* [1968], the release wave reflects from the downrange sample surface (geometry A).

Experiment Data Records

This supplement includes the calibrated particle velocity data traces from each impact experiment. The data records are presented for the time period up until the gauge breaks. Gauge locations are specified as distances from the front of the first ice disc in the target assembly. The primary error on the measurement of the gauge location is the measurement of the thickness of the ice discs and are estimated to be about 0.025 mm.

Thick targets (> 10 mm) are designed to measure the primary shock wave profile. Thin targets (≤ 10 mm) are designed to measure both the shock wave and release wave, reflected from the rear of the target. In this geometry, the release wave produces an increase in particle velocity.

All experiments have a 0.7 mm polycarbonate buffer disc at the front of the target, which preserved contact between the first gauge and the first ice disc. All shots used solid polycarbonate projectiles. The buffer disc thickness was comparable to the width of the shock front, and the particle velocity at the first ice disc was determined by the impedances of the polycarbonate and ice rather than a symmetric polycarbonate impact. This is confirmed with shots #1037 and #1038 [*Stewart and Ahrens*, in preparation], with and without a polycarbonate buffer, where the same peak particle velocity was recorded in each experiment.

Experiments with impact velocities < 350 m s^{-1} (I44-I45) are compressed gas (He) shots. Experiments with higher impact velocities (#1043-1047) are driven by propellant (IMR4350). The uncertainties shown in the loading path figures are 1σ.

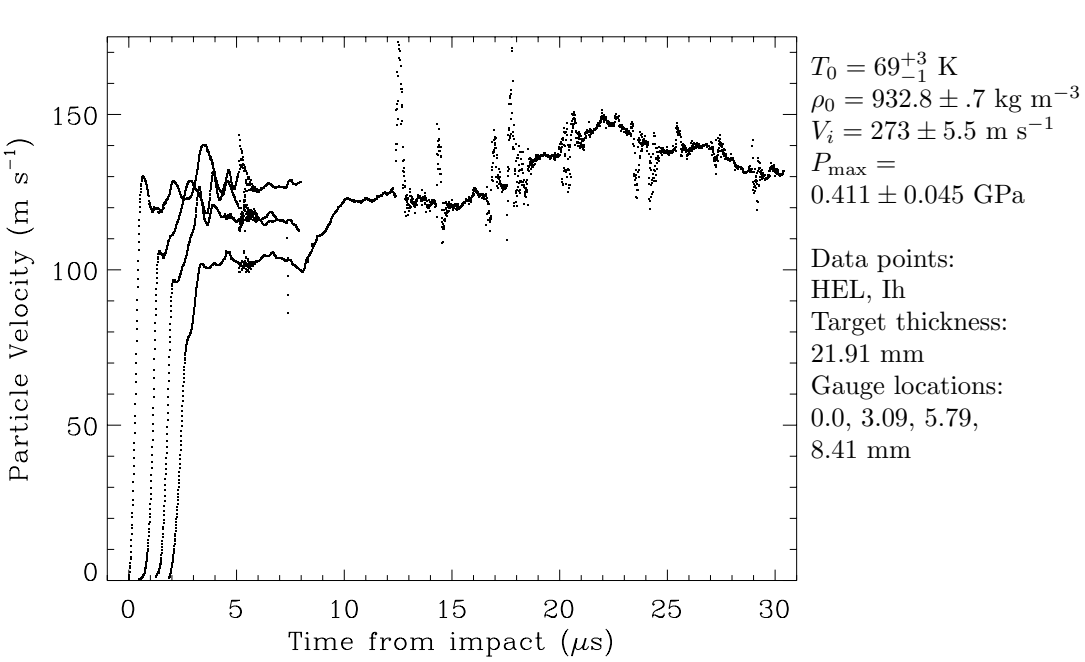

Figure S2: Data record.

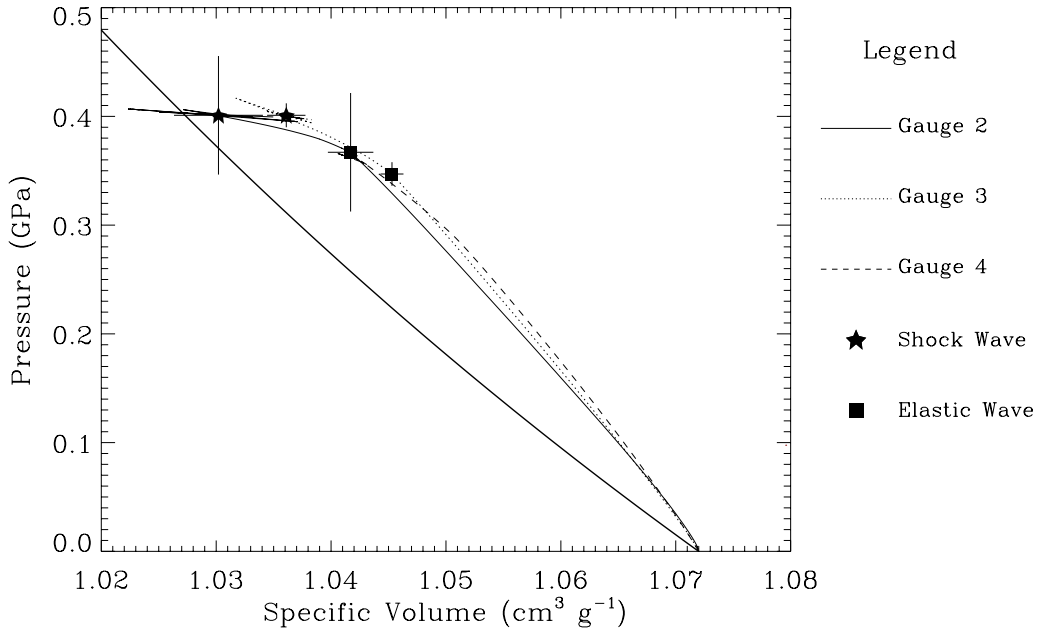

Figure S3: Loading path.

Notes: Peak pressures just above HEL achieved. Propagating shock wave was not steady and decays to an elastic wave by arrival at 4$^{\text{th}}$ gauge. 4$^{\text{th}}$ gauge also displays a release profile which may be a combination of release from sides and rear of target. Velocity resolution of oscilloscope is ~ 1.7 m s^{-1}.

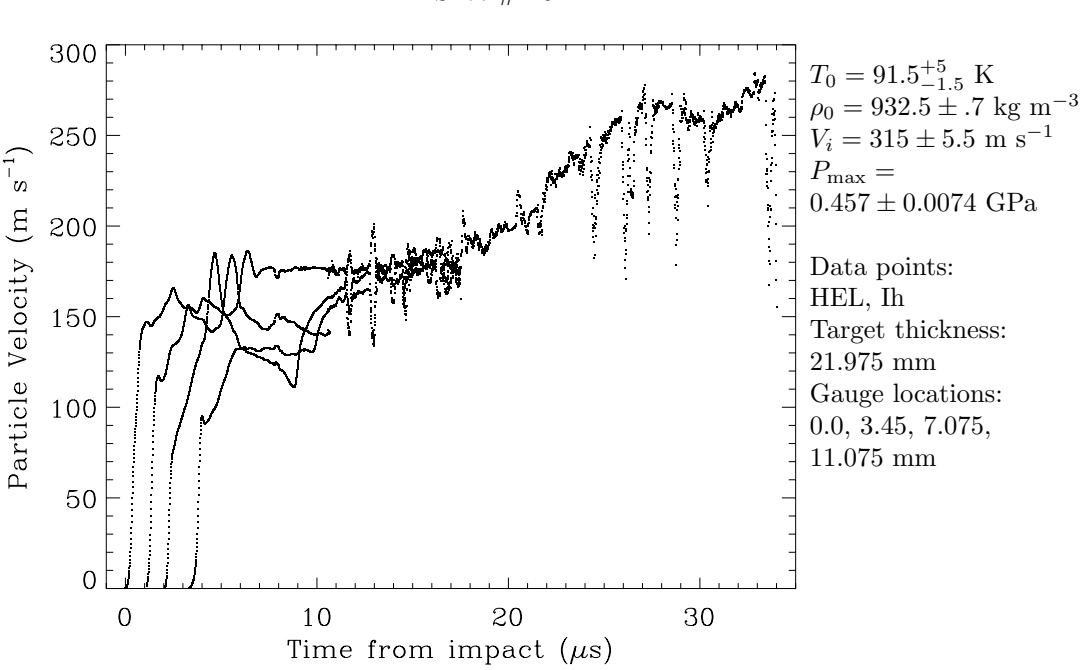

Figure S4: Data record.

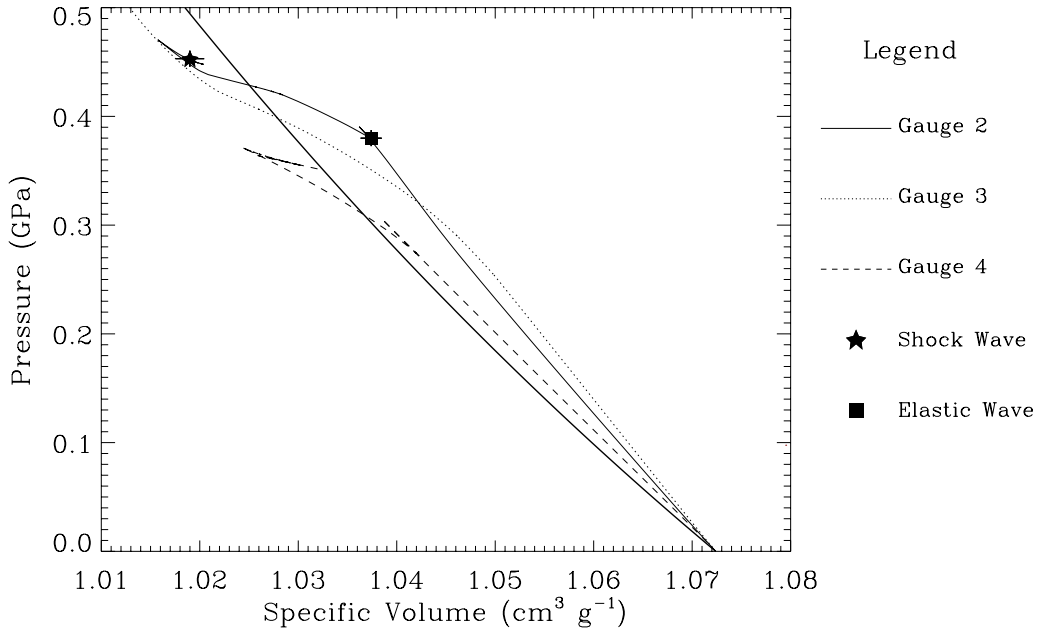

Figure S5: Loading path.

Notes: Peak pressures just above HEL achieved. Final shock wave is not steady. There was a space between the 2$^{\text{nd}}$ and 3$^{\text{rd}}$ ice discs in the target assembly. Motion of the free surface between discs #2 and 3 produced a ~ 30 m s^{-1} peak to peak oscillation of gauge 3. The space partially releases the shock wave, so the wave arrival at the 4$^{\text{th}}$ gauge has decayed to the Hugoniot Elastic Limit. The spike wave feature appears to reflect from the gap boundary back to the 2$^{\text{nd}}$ and 1$^{\text{st}}$ gauges, propagating at the sound speed in the shocked state. Only the shock propagation time from the 1$^{\text{st}}$ to 2$^{\text{nd}}$ gauge is used for Hugoniot data points. Release from the rear of the target is recorded in gauges 4 and 3. Velocity resolution of oscilloscope is about 1.3 m s^{-1}.

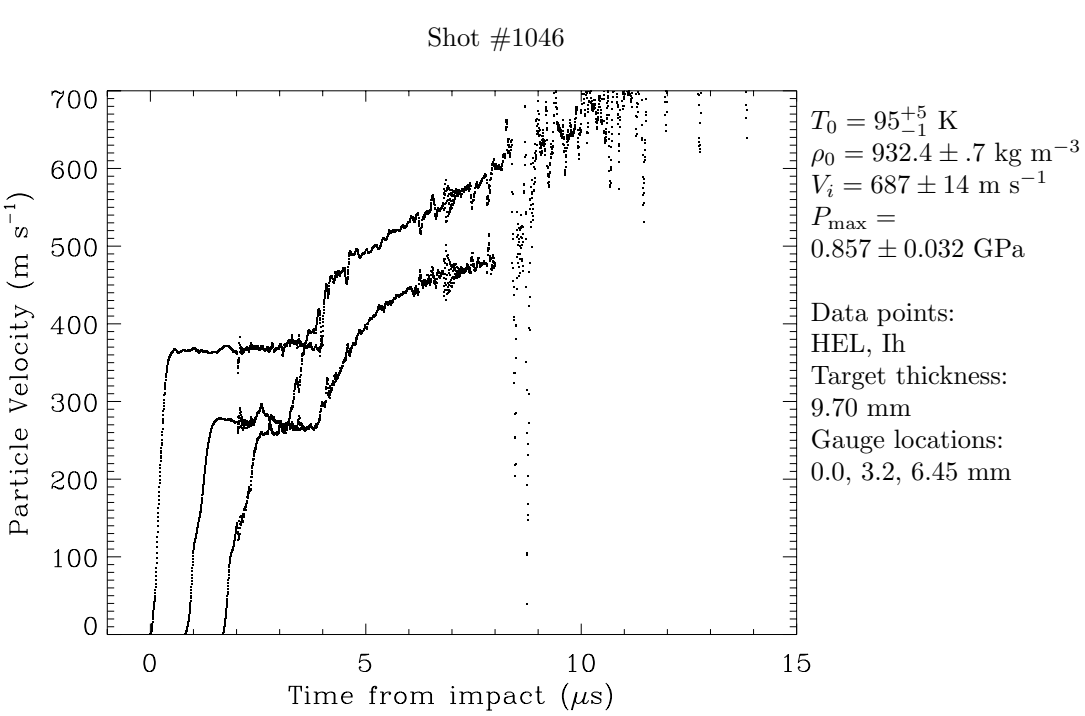

Figure S6: Data record.

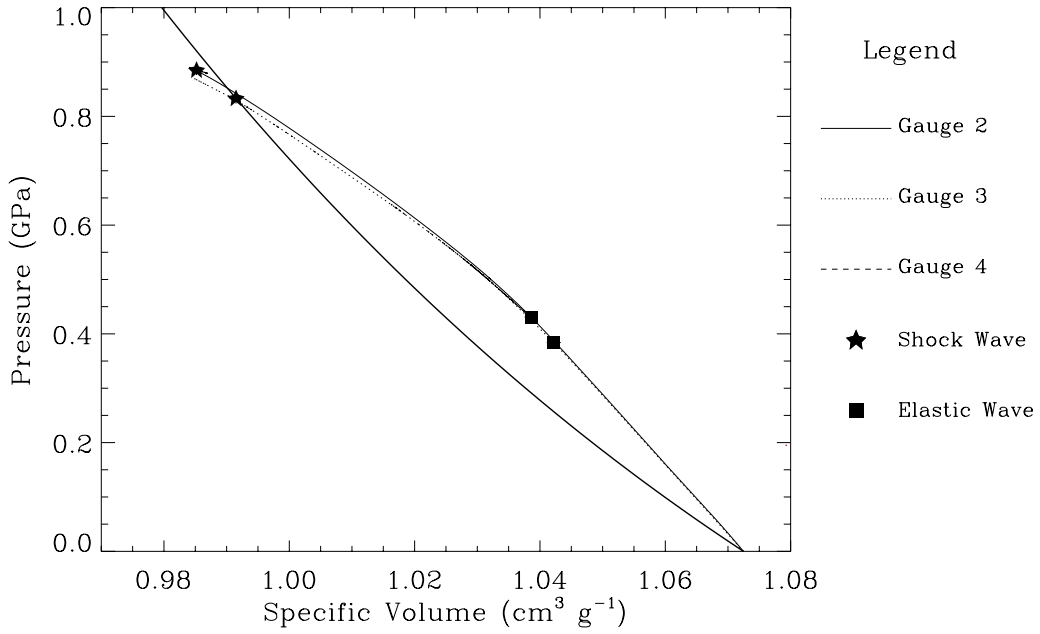

Figure S7: Loading path.

Notes: This impact initiated a wave with peak pressures above the ice Ih shock pressure which propagates to gauges 2 and 3. But the wave velocity for a transformation to a higher pressure phase was too slow to propagate to the 2$^{\text{nd}}$ gauge during the time frame of the experiment. The release from the rear arrives before the transformation wave. Thus, only a HEL and Ih shock wave are detected in gauges 2 and 3 before release from the rear of the target. Ideal release curves are recorded in the 2$^{\text{nd}}$ and 3$^{\text{rd}}$ gauges. Velocity resolution of the oscilloscope is about 1.9 m s^{-1}.

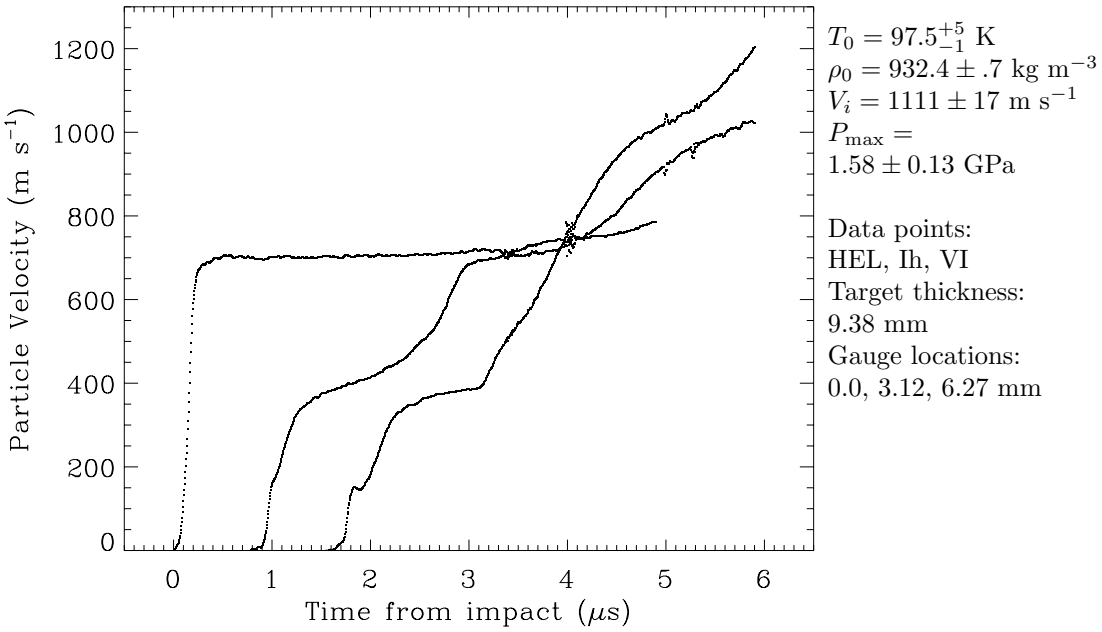

Figure S8: Data record.

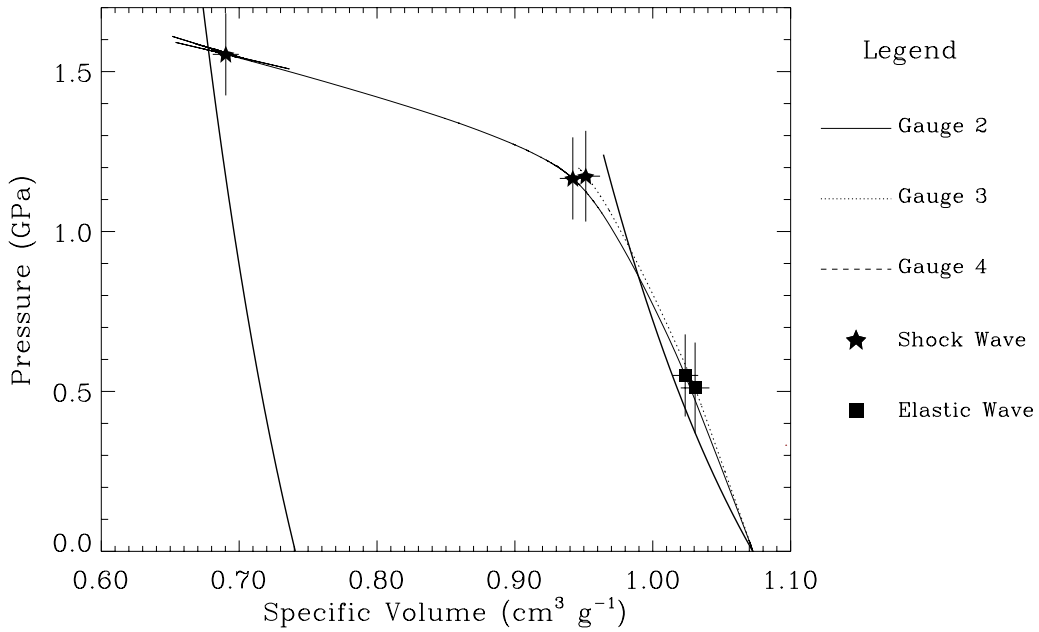

Figure S9: Loading path.

Notes: This shot produced a transformation shock to the ice VI structure. The three-wave structure is clear in the 2$^{\text{nd}}$ gauge. The release wave from the rear of the target reaches gauge 3 before the ice VI transformation wave arrives. Velocity resolution of the oscilloscope is about 5.4 m s^{-1}.

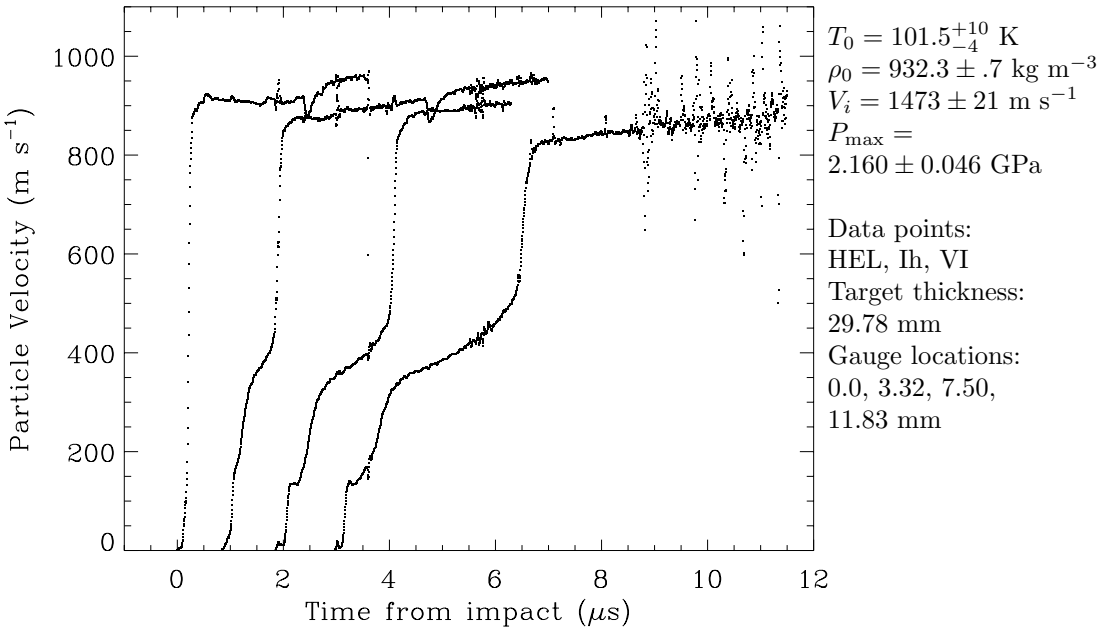

Figure S10: Data record.

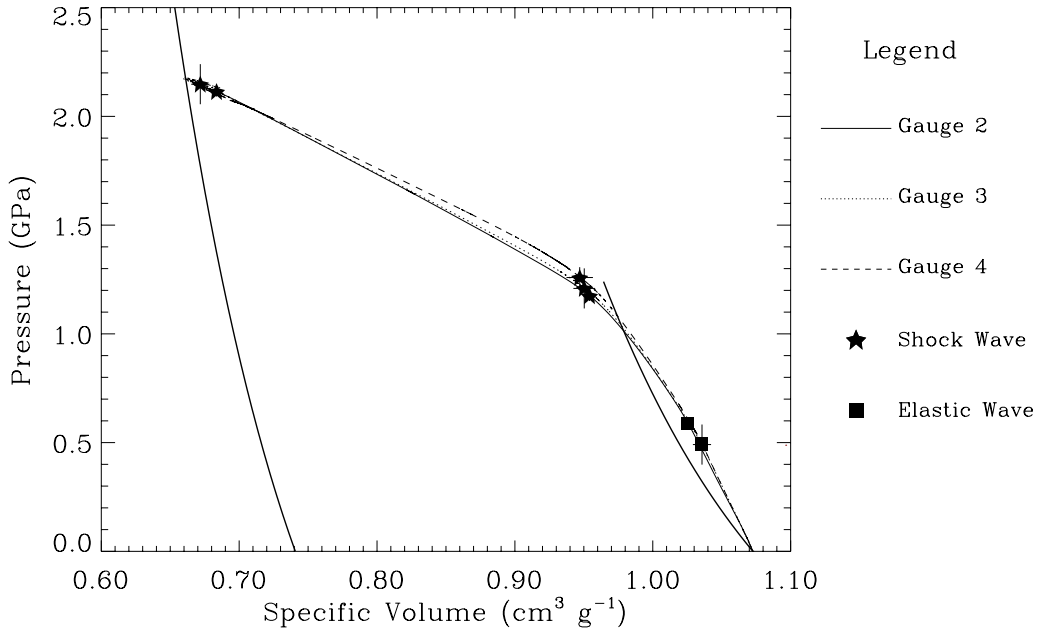

Figure S11: Loading path.

Notes: This shot produced a transformation shock to the ice VI structure. The three-wave structure is clear in the 2$^{\text{nd}}$ gauge. The three-wave structure is clear in the 2$^{\text{nd}}$, 3$^{\text{rd}}$ and 4$^{\text{th}}$ gauges. The wave has decayed a little by the arrival at the fourth gauge and this peak shock state is not part of the ice shock Hugoniot dataset. Velocity resolution of the oscilloscope is about 6.6 m s^{-1}.

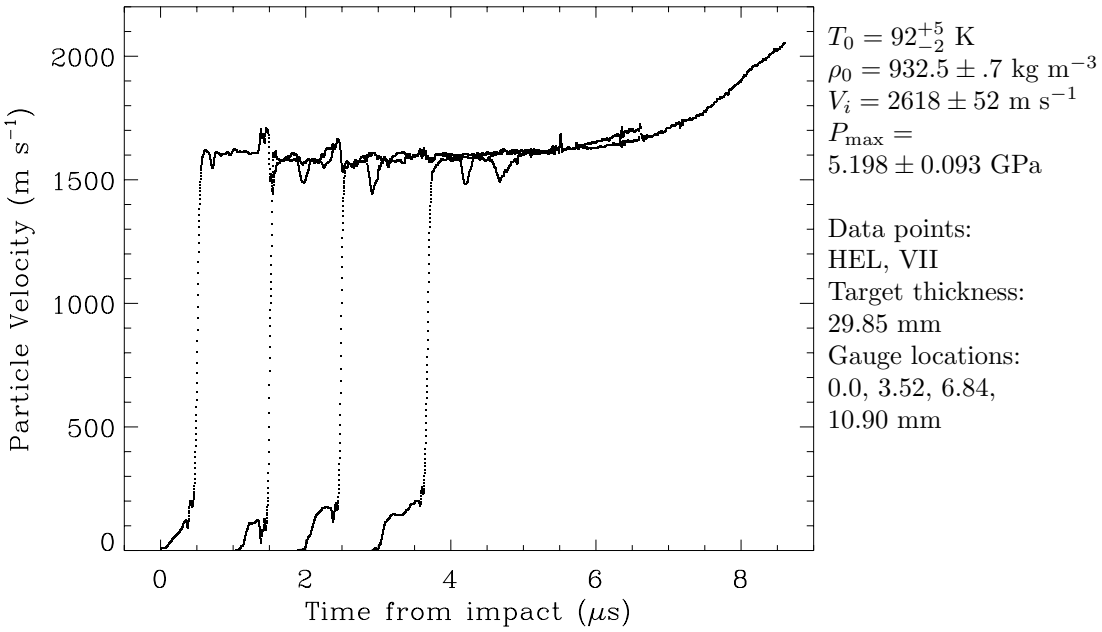

Figure S12: Data record.

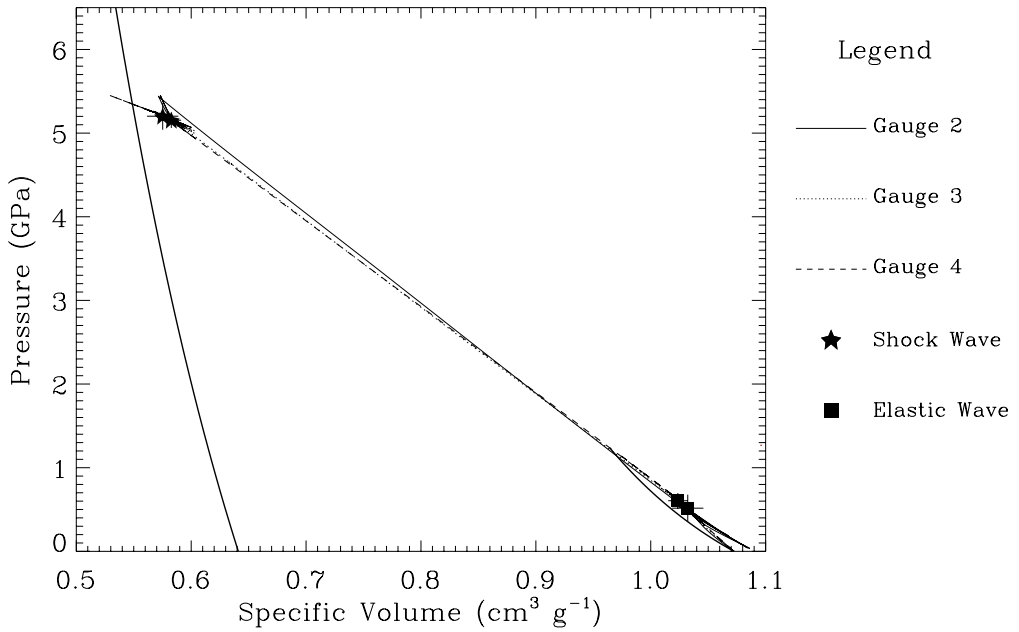

Figure S13: Loading path.

Notes: This impact drove a transformation to the ice VII structure. The shock wave split into a two-wave structure: the HEL wave and ice VII transformation shock. The loading profile is close to the ideal shape: a straight line from the initial to the final P,V state. Since the ice VII transformation shock velocity (3.4-3.5 km s^{-1}) is nearly the HEL wave speed, stronger shocks will over drive the HEL. The knee in the 1st gauge implies that the impact was not perfectly normal to the target. This probably resulted in a slightly higher than ideal peak pressure, since the shock wave propagated on top of this initial wave arrival. The imperfect impact also influenced the shape of the HEL wave, but did not affect the wave speed calculations. Velocity resolution of oscilloscope is about 13.8 m s^{-1}.

References

Anderson, G. D. (1968), The equation of state of ice and composite frozen soil material, *Research Report 257*, Cold Regions Res. & Eng. Lab., Hanover, NH.

Davies, F. W., and E. A. Smith (1994), High pressure equation of state investigation of rocks, *Technical Report DNA-TR-94-1*, Defense Nuclear Agency, Ktech Corporation, Albuquerque, NM.

Gaffney, E. S., and E. A. Smith (1994), HYDROPLUS experimental study of dry, saturated, and frozen geological materials, *Technical Report DNA-TR-93-74*, Defense Nuclear Agency, Ktech Corporation, Albuquerque, NM.

Larson, D. (1984), Shock-wave studies of ice under uniaxial strain conditions, *J. Glaciology*, *30*(105), 235–240.

*S. T. Stewart, now at: Department of Earth and Planetary Sciences, Harvard University, 20 Oxford St., Cambridge, MA 02138. Email: sstewart@eps.harvard.edu

T. J. Ahrens, Division of Geological and Planetary Sciences, California Institute of Technology, MC 252-21, Pasadena, CA 91125. Email: tja@gps.caltech.edu

(Received _____)

Paper number .

STEWART AND AHRENS: SHOCK PROPERTIES OF H_2O ICE: AUXILIARY MATERIAL

STEWART AND AHRENS: SHOCK PROPERTIES OF H_2O ICE: AUXILIARY MATERIAL

STEWART AND AHRENS: SHOCK PROPERTIES OF H_2O ICE: AUXILIARY MATERIAL

STEWART AND AHRENS: SHOCK PROPERTIES OF H_2O ICE: AUXILIARY MATERIAL

STEWART AND AHRENS: SHOCK PROPERTIES OF H_2O ICE: AUXILIARY MATERIAL

STEWART AND AHRENS: SHOCK PROPERTIES OF H_2O ICE: AUXILIARY MATERIAL

STEWART AND AHRENS: SHOCK PROPERTIES OF H_2O ICE: AUXILIARY MATERIAL

STEWART AND AHRENS: SHOCK PROPERTIES OF H_2O ICE: AUXILIARY MATERIAL

STEWART AND AHRENS: SHOCK PROPERTIES OF H_2O ICE: AUXILIARY MATERIAL

STEWART AND AHRENS: SHOCK PROPERTIES OF H_2O ICE: AUXILIARY MATERIAL

STEWART AND AHRENS: SHOCK PROPERTIES OF H_2O ICE: AUXILIARY MATERIAL

STEWART AND AHRENS: SHOCK PROPERTIES OF H_2O ICE: AUXILIARY MATERIAL

STEWART AND AHRENS: SHOCK PROPERTIES OF H_2O ICE: AUXILIARY MATERIAL

STEWART AND AHRENS: SHOCK PROPERTIES OF H_2O ICE: AUXILIARY MATERIAL

STEWART AND AHRENS: SHOCK PROPERTIES OF H_2O ICE: AUXILIARY MATERIAL

STEWART AND AHRENS: SHOCK PROPERTIES OF H_2O ICE: AUXILIARY MATERIAL

STEWART AND AHRENS: SHOCK PROPERTIES OF H_2O ICE: AUXILIARY MATERIAL

STEWART AND AHRENS: SHOCK PROPERTIES OF H_2O ICE: AUXILIARY MATERIAL

STEWART AND AHRENS: SHOCK PROPERTIES OF H_2O ICE: AUXILIARY MATERIAL

STEWART AND AHRENS: SHOCK PROPERTIES OF H_2O ICE: AUXILIARY MATERIAL

STEWART AND AHRENS: SHOCK PROPERTIES OF H_2O ICE: AUXILIARY MATERIAL